First absolute measurements of fast-ion losses in the ASDEX Upgrade tokamak

M. Rodriguez-Ramos 1,2), M. Garcia-Munoz 1,2), M.C. Jimenez-Ramos 2), J. Garcia Lopez 1,2), J. Galdon-Quiroga 1,2), L. Sanchis-Sanchez 1,2), J. Ayllon-Guerola 2), M. Faitsch 3), J. Gonzalez-Martin 2), A. Hermann 3), P. de Marne 3), J.F. Rivero-Rodriguez 2), B. Sieglin 3), A. Snicker 3) and the ASDEX Upgrade Team‡ 3)

1) Department of Atomic, Molecular and Nuclear Physics. University of Sevilla, Sevilla, Spain
2) CNA (U. Sevilla, CSIC, J. de Andalucia), Sevilla, Spain
3) Max-Planck-Institut für Plasmaphysik, Garching, Germany

E-mail: mrodriguez67@us.es

Abstract.

A new diagnostic technique that allows to obtain absolute fluxes of fast-ion losses measured with absolutely calibrated scintillator based Fast-Ion Loss Detectors (FILD) is presented here. First absolute fluxes of fast-ion losses have been obtained in the ASDEX Upgrade tokamak. For this purpose, an instrument function that includes the scintillator efficiency, collimator geometry, optical transmission and camera efficiency has been constructed. The scintillator response to deuterium ions in the relevant energy range of fast-ions has been characterised using a tandem accelerator. Absolute flux of Neutral Beam Injection (NBI) prompt losses has been obtained in magnetohydrodynamic (MHD) quiescent plasmas. The temporal evolution of the heat load measured with FILD follows that measured at the FILD entrance obtained with an Infra-Red (IR) camera looking at the FILD detector head. ASCOT simulations are in good agreement with the absolute heat load of NBI prompt losses measured with FILD.

‡ For authors' list, see U. Stroth et al., Nucl. Fusion 53, 104003 (Year: 2013).

1. Introduction

In fusion devices, fast-ions generated by external heating systems: Neutral Beam Injection (NBI), Ion Cyclotron Resonance heating (ICRH) and fusin born alpha particles constitute an essential source of energy and momentum. There are several fast-ion transport mechanisms that can have an impact on the performance of the heating systems affecting their efficiency and even threatening the device integrity [1, 2]. Although losses caused by Coulomb collisions and equilibrium geometry are rather well known and controllable, fast-ions losses induced by MHD fluctuations are not yet fully understood [3]. Experimentally, a good understanding of the fast-ion transport mechanisms can be obtained from direct measurements of fast ion losses at the plasma edge using scintillator based Fast-Ion Loss Detectors (FILD) [4, 5]. FILD systems act like magnetic spectrometers dispersing the escaping ions onto a scintillator by means of a 3D collimator with their impact points depending on their local pitch-angle and gyroradius, see Fig.1-(a).

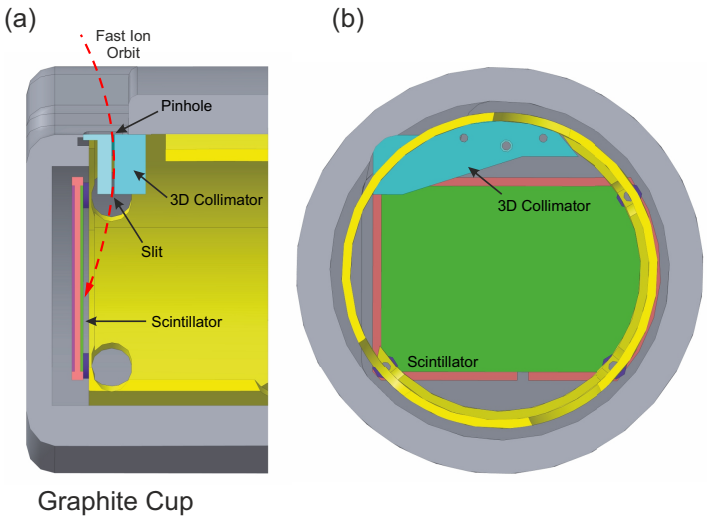

Figure 1. Schematic of the FILD scintillator housing: (a) Side view showing the collimator structure (blue), the scintillator plate (green) and one escaping ion trajectory impinging on the scintillator (red). (b) Front view of the FILD1 head showing the collimator (pinhole+slit) structure.

The light emitted from the scintillator is transmitted through an optical system and imaged by a camera and an array of photomultipliers. Although FILD systems are working on virtually all fusion devices, inherent limitations to the FILD technique, e.g. complicated scintillator response to charge particles, prevent the community to make reliable assessments on the absolute fast-ion losses caused by MHD fluctuations in fast-ion velocity-space. This is, indeed, of crucial importance to validate codes (physics understanding) as well as to improve our prediction capabilities towards future devices such as ITER or DEMO. The new diagnostic technique presented here should allow to obtain absolute fluxes of escaping ions in fast-ion velocity-space. In this work, we describe the procedure we have followed to calibrate the FILD systems of the AUG tokamak. Absolute values of fast-ions losses obtained with different heating system (NBI and ICRH) are presented. After an introduction given in section I, the calibration procedure followed to obtain the instrument function is described in section II. The scintillator efficiency to relevant ions, the weighting function used to obtain absolute values of escaping ions in velocity-space as well as to construct the instrument function are presented. This paper ends with a comparison with ASCOT NBI losses and a summary section.

2. Calibration

2.1. Characterization of scintillator efficiency in a tandem accelerator

The characterization of the efficiency ϵ of the scintillator material installed in the AUG FILD systems ($SrGa_2S_4 : Eu^{2+}$ [6]) has been carried out using the 3 MV tandem accelerator of the Spanish National Center of Accelerators (CNA) [7]. The ion luminescent efficiency of the phosphor $SrGa_2S_4 : Eu^{2+}$ (TG-Green) was analyzed when irradiating with $10^{10} - 10^{11}$ $ions/s \cdot cm^2$ with energies between 0.5-3 MeV at room temperature. A spectrometer QE65000 (Ocean Optics Inc.) was used to characterize the spectral response of the scintillator, see Fig.2.

The measured spectra present a broad peak at 539 nm (2.3 eV with an emission width of 0.20 eV) and short decay time ≈ 490 ns. The composition of the sample and the physical thickness (around 9 μm) were determined by Rutherford Backscattering Spectrometry (RBS) using protons at 3 MeV [8].

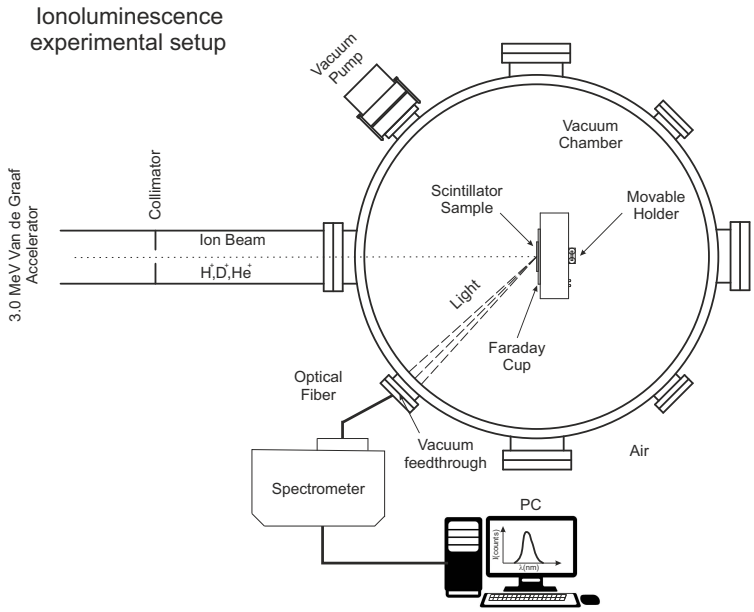

Figure 2. A schematic diagram of the experimental IBIL (ion beam induced luminescence) setup at CNA showing the scintillator and the photon detector as well as the incident ion beam and light acquisition systems.

The conversion between the spectrometer signal and photon yield was made calibrating the optical acquisition system with a HL-2000-CAL Tungsten Halogen Calibration Standard light source. Fig.3 shows the measured absolute ionoluminescence yield of the material under study as a function of the ion energy for deuterons in the energy range between 0.5 and 3.0 MeV. A good agreement with the Birk's law [9] is found over the entire energy range available, at present, at the CNA accelerator. The TG-Green photon yield for deuterium ions in this energy range can be reproduced by Birk's formula with an accuracy of about 10%. At energies below 100 keV, the Birk's law predicts a linear dependency of the photon yield with the energy of the impinging charge particles [10]. The Birk's law predicts, thus, for the AUG NBI injection energy, an efficiency ϵ, between $2{\times}10^3$ and $8{\times}10^3$ photons/ion.

Measurements of the scintillator efficiency at energies below 100 keV are planned and will be the subject of a future work as some modifications in the accelerator setup are necessary and are currently being designed.

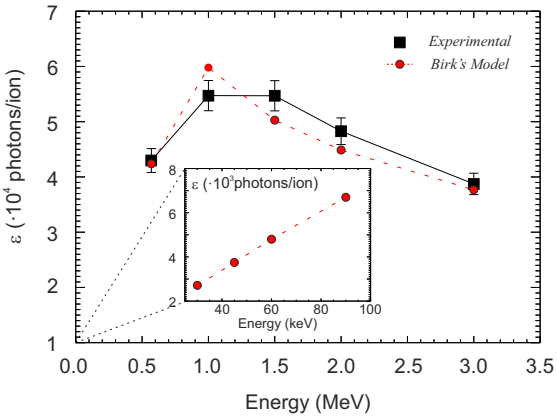

Figure 3. Experimental (black) and estimated by Birk's model (red) photon yield for deuterons in the $SrGa_2S_4 : Eu^{2+}$ scintillator at room temperature.

2.2. The FILD weighting function

FILD system works as magnetic spectrometer making use of a 3D collimator and the tokamak magnetic field to disperse the measured escaping ions on a scintillator plate depending on their energy and pitch-angle. The detector head is protected against heat load with a graphite heat shield, see Fig.1-(b). The measurable velocity-space range on the scintillator plate depends on the 3D geometry of the entire head, a three-dimensional structure (pinhole + slit entrance). To estimate the ion flux impinging to the head, a weighting function similar to that obtained for confined ions measured with FIDA [11] has been developed. The collimator factor f_{col}, defined as the ratio between the number of ions reaching the collimator pinhole (which can be related to the losses at the first wall) and the number of ions that hit the scintillator plate has been calculated in the scintillator fast-ion velocity-space. For this purpose, Monte Carlo simulations with the orbit-tracing FILDSIM code [12] have been performed. Given the initial distribution in velocity-space for the incoming ions reaching the pinhole, FILDSIM allows us to obtain the distribution generated in the scintillator plate.

FILDSIM simulates ion trajectories started at the detector pinhole with different gyroradii and pitch angles. The code assumes that the local magnetic field in the volume of the probe head is constant and the orbits followed by the ions are helixes. The code provides the location where each particle hits the scintillator plate. The code provides the location where each particle hits the scintillator plate. Results show that the actual collimator transmission for the AUG FILD systems is approx 1-3 % of the particles hitting the aperture, see Fig.4-(a). Fig.4-(b) shows the efficiency of the scintillator to deuterium ions with a magnetic field of 1.7 T. To reproduce the velocity-space distribution measured at the scintillator plate, using a simulated escaping ion distribution at the pinhole, a weighting function $W(E, \Lambda)$ that depends on the energy and the pitch angle of the particles has been constructed and is shown in Fig.4-(c).

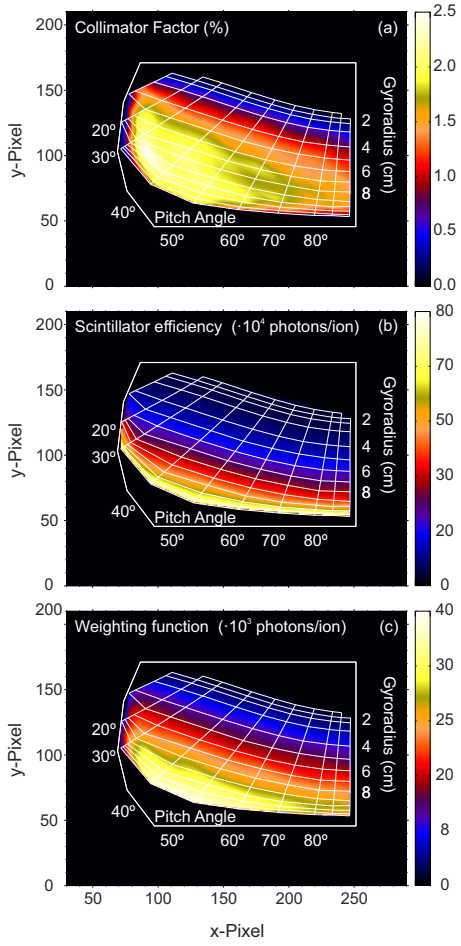

Figure 4. (a) Collimator factor, (b) scintillator efficiency and (c) weighting function for the AUG FILDs.

The lost ion flux at the scintillator can be related to that at the pinhole (first wall) by means of the weighting functions through the following expression:

$$\Gamma^{Sim}_{scintillator} = \Gamma^{Sim}_{pinhole} \times \underbrace{f_{col}(E,\Lambda) \times \epsilon(E)}_{W(E,\Lambda)} \quad (1)$$

2.3. Characterization of the optical path and efficiency of light acquisition systems

The light transmission of the FILD optical system has been estimated using an integrating sphere (Labsphere Unisource 1200) with a light source (at current 6.5 A) of known radiance working at 15.6 mV. The detector head was replaced by the integrating sphere, obtaining a well known and uniform light source. The light is transmitted through a series of lenses to an optical bundle that transfers the light to the CCD camera, see Fig.5.

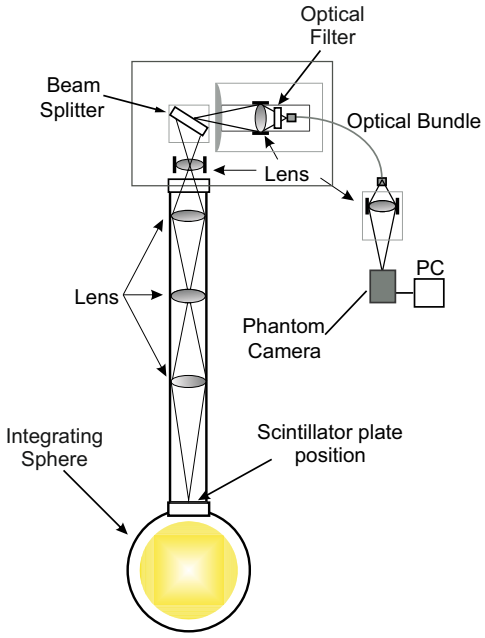

Figure 5. Setup used to calibrate the optical path system of FILD1 detector at ASDEX Upgrade.

A bandpass filter was placed in front of the optical bundle (maximum coefficient of transmission about 38 % with a centroid at a wavelength of 525 nm and with a FWHM=3.7 nm) to restrict the photon emission to the scintillator spectra emission.

The quantification of the absolute photon flux Φ_{IS} (number of photons per unit time, and per unit area) emitted by the sphere port in terms of spectral radiance $L_{e,\lambda}(\lambda)$ (see Fig.6) and transmission coefficient $T(\lambda)$ of the optical filter was obtained following the expression:

$$\Phi_{IS} = 4\pi \int L_{e,\lambda}(\lambda) \cdot T(\lambda) d\lambda \approx 7.83 \cdot 10^{18} \, \frac{photons}{s \cdot m^2} \tag{2}$$

The light pattern produced by the integrating sphere was measured by the FILD camera with an exposure time of Δt =42 ms and was later compared to the luminosity of the scintillator response to fast-ions. The exposure time Δt of the camera has been selected to obtain an intensity of the pixels approximately equal to the half dynamic range of the camera. The pixel intensity of the calibration frame ($I_{IS} \approx 170$ counts), and the integrated photon flux Φ_{IS} allows to obtain the following calibration factor for each pixel:

$$\xi = \frac{\frac{I_{IS}}{\Delta t}}{\Phi_{IS} \cdot S_\Omega} \approx 1.0 \cdot 10^{-10} \times I_{IS} \, \frac{Counts}{photons} \tag{3}$$

where S_Ω is the area from the integrating sphere port viewed by a pixel of the CCD chip. This expression relates the counts from the CCD frame with the number of photons hitting the sensor of the camera.

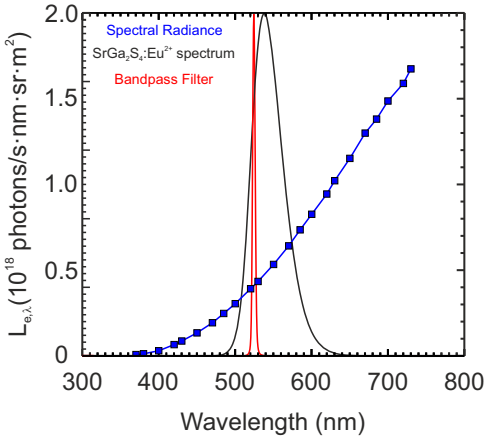

Figure 6. Wavelength dependence of the spectral radiance of the integrating sphere (blue). Normalized bandpass filter transmission coefficient (red) and normalized $SrGa_2S_4 : Eu^{2+}$ ionoluminscence spectrum (black).

2.4. The FILD instrument function

The calibration of the light acquisition system and the weighting function of the AUG FILD has been used to construct an instrument function that converts the experimental fast-ion loss signals into absolute fluxes for each (p,q) pixel. The equation is introduced as follows:

$$\Gamma_{pinhole}^{Exp} = \frac{1}{S_{pinhole} \cdot \Delta t} \int \int_{\Omega(E,\Lambda)} \frac{I(E,\Lambda)}{W(E,\Lambda) \times \xi(E,\Lambda)} dE d\Lambda \tag{4}$$

where $I(E,\Lambda)$ is the intensity of the (p,q) pixel in the velocity-space, $S_{pinhole}$ the surface area of the pinhole and Δt the exposure time of the camera during the discharge. The energy and pitch angle resolution of the detector defines the region of integration (Ω) assuming a bidimensional gaussian distribution of the losses in the velocity-space [4].

3. Results

The instrument function obtained here has been applied to fast-ions signals obtained in NBI and ICRH heated plasmas using the FILD1 system. An infrared camera [13] has been used to measure the heat load on the detector head. The absolute fluxes of fast-ion losses have been obtained in an AUG discharge (# 30810) with B_t = -2.35 T , I_p = 1.0 MA and q_{95} = 3.8. An overview of the most relevant plasma parameters is shown in Fig.7. The absolute fluxes obtained here with FILD1 have been compared with IR measurements of the detector head.

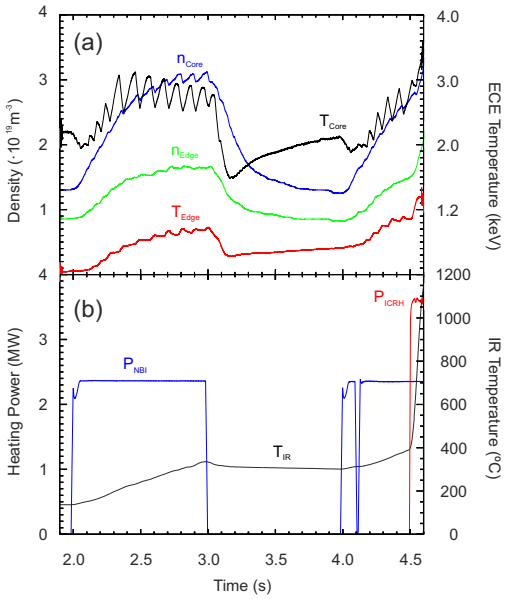

Figure 7. AUG#30810. Overview of the discharge: a) Left axis: Interferometer line integrated density in the core (blue) and in the edge at $\rho_{pol} \approx 0.8$ (green). Right axis: Electron temperature in the core (black) and in the edge at $\rho_{pol} \approx 0.95$ (red) electron temperature. b) Left axis: Time trace of external heating power and right axis: FILD apperture temperature.

Fig.8 shows the temperature of the FILD1 head due to heat load.

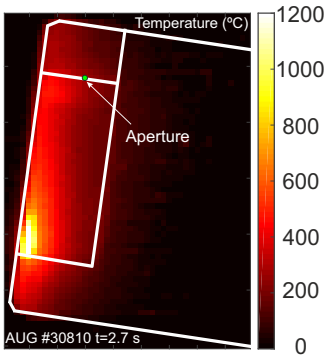

Figure 8. AUG#30810. 2D image of the temperature of the FILD1 detector head. The green dot indicates the position of the aperture.

In Fig.9-(a), the velocity-space of the NBI prompt losses measured with FILD1 is shown. A clear spot at a gyroradius of 2.8 cm and a pitch angle of $\approx 55°$ corresponding to 60 keV (main NBI3 injection) is clearly visible. The Birks model predicts that the TG-Green response for deuterium ions at 60 keV is about 4900 photons/ions at room temperature.

The weighting function presented in Fig.4-(c) allows us to calculate the absolute flux and heat load on the detector aperture. The temporal evolution of the fast-ion heat load on the detector aperture considering that the scintillator is kept at room temperature is presented in Fig.9-(b) and Fig.9-(c) together with the heat load measured on the same position by the IR camera.

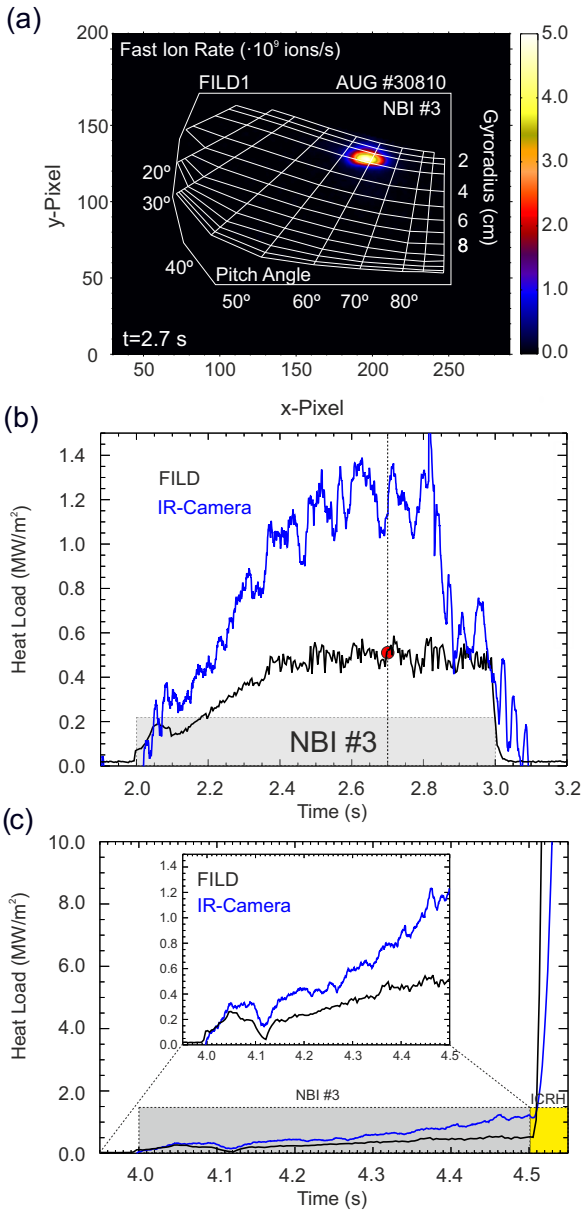

Figure 9. AUG#30810. (a) Fast-ion rate on the scintillator plate. The visible spot is a typical prompt-loss signal. (b) Temporal evolution of the absolute prompt losses measured with FILD1 (black) and IR camera (blue) during a NBI phase. The heat load provided by ASCOT at the pinhole of the FILD1 head is shown (red dot) at t=2.7 s. (c) NBI+ICRH phase.

A clear match between the temporal evolution of both signals is obtained with the infrared signal somewhat above the FILD heat load due to the thermal plasma contribution. In this discharge, the heat load on the first wall arising from the NBI prompt losses have been modeled with the full orbit code ASCOT [14]. To make realistic simulations, the temperature and density profiles for the discharge #30810 have been used to calculate the density of NBI deposited ions for the time point analyzed here, t =2.7 s, see Fig.10.

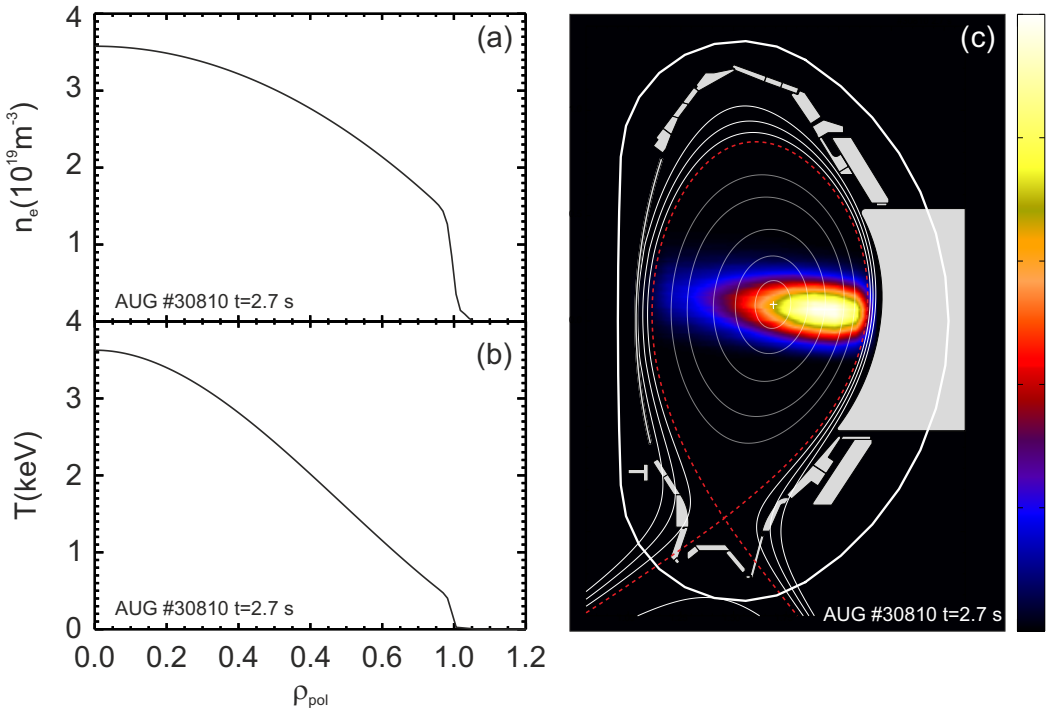

Figure 10. AUG#30810 kinetic profiles: Density (a) and temperature (b) profiles used in simulations for discharge AUG #30810 at t = 2.7 s. The figure c) shows a R-z image of the simulated birth density with the selected profiles.

In these simulations, 5×10^5 Monte Carlo markers were followed until they hit a plasma facing component or are slowed down to the background thermal energy. For each lost marker, ASCOT provides the (R,φ,Z) coordinates where each marker hits the plasma facing components, as well as its energy and pitch angle at the impact location.

A typical trajectory of fast-ion measured with the AUG FILD1 (located just above the midplane at z=0.30 m and a radial position R=2.161 m) is plotted in Fig.11.

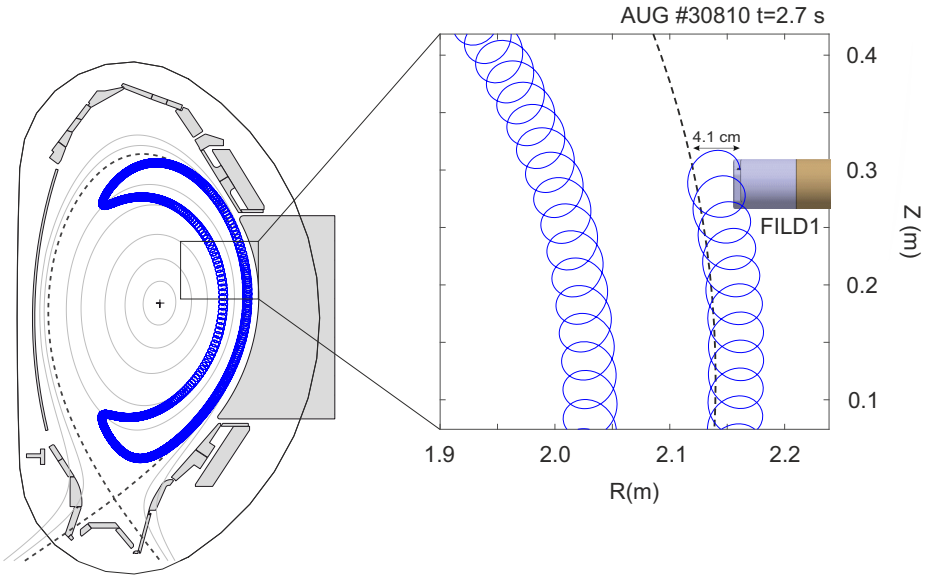

Figure 11. AUG#30810. Poloidal view of one banana orbit (blue) with E= 60 keV and $\Lambda = 55$ °. FILD1 position at AUG tokamak showing the distance between the detector and the separatrix (shown in black and dashed).

A map of the heat load (in kW/m^2) obtained by making a 2D histogram of the losses in the toroidal-poloidal plane is presented in Fig.12.

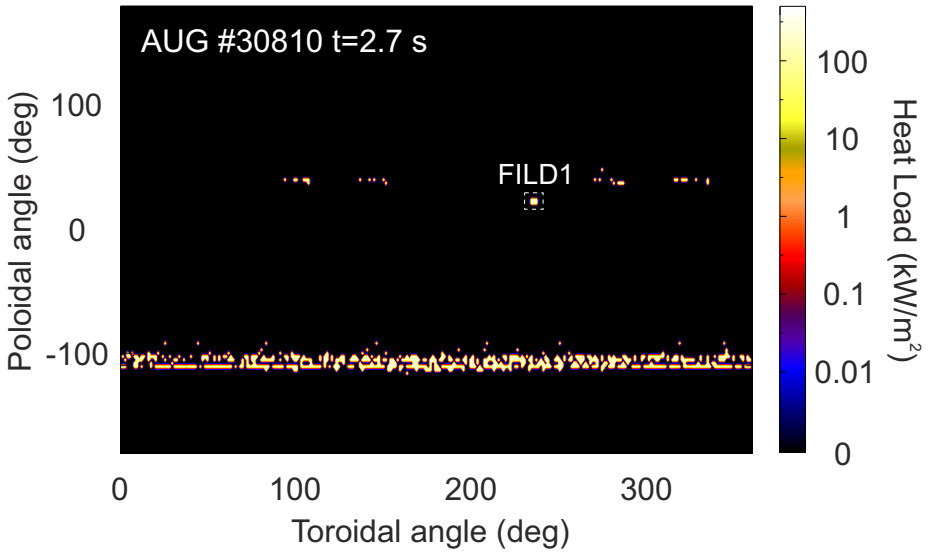

Figure 12. AUG#30810. Wall power load due to NBI #3 at t=2.7 s obtained with ASCOT.

A satisfactory agreement of the absolute flux obtained here with FILD1 and ASCOT simulations has been found with the fast-ion heat load on the detector head around 450-500 kW/m^2. This heat load is consistent with that obtained previously with IR cameras at the AUG [15] tokamak and in a NBI heated DIII-D discharge with similar magnetic fields and plasma parameters [16].

4. Summary

The absolute flux of NBI prompt losses and ICRH losses measured by a FILD system in the AUG tokamak has been obtained for the first time. A FILD instrument function that includes the scintillator efficiency, collimator geometry, optical transmission and camera efficiency allowed to estimate the absolute flux of ions in FILD velocity-space. The temporal evolution of the heat load measured with FILD follow that measured with an IR camera looking at the detector head. The heat load measured with the IR camera is always somewhat above that measured with FILD due to the thermal plasma contribution. ASCOT simulations of the heat load on the detector head are in fairly good agreement with the absolute heat load obtained with FILD measurements. The FILD weighting function developed here will allow to invert the real velocity-space of the fast-ion distribution at the tokamak first wall/detector entrance [17]. Absolute values of fast-ion losses in velocity-space will certainly help validating fast-ion transport codes and thus improving our abilities to make predictions toward ITER and other future fusion devices.

5. Acknowledgments

This research was supported in part by the Spanish Ministerio de Economia, Industria y Competitividad (RYC-2011-09152, FIS2015-69362-P and ENE2012-31087) FEDER/UE, the Marie Curie FP7 Integration Grant, PCIG11-GA-2012- 321455, within the framework of the EUROfusion Consortium and has received funding from the Euratom research and training programme 2014–2018 under grant agreement number

633053 and the V Plan propio de la Universidad de Sevilla (VPPI-US). The views and opinions expressed herein do not necessarily reflect those of the European Commission. We are grateful to C. Bravo Falcon for the set-up model in CAD.

References

[1] Duong H H and Heidbrink W W 1993 Confinement of fusion produced MeV ions in the DIII-D tokamak *Nucl. Fusion.*, **33** 749

[2] Fasoli A *et al* 2007 Chapter 5: Physics of energetic ions *Nucl. Fusion.*, **47** S264

[3] Garcia-Munoz M *et a*l 2009 MHD induced fast-ion losses on ASDEX Upgrade *Nucl. Fusion.*, **49** 085014

[4] Garcia-Munoz M, Fahrbach H -U, Zohm H and the ASDEX Upgrade Team 2009 Scintillator based detector for fast-ion losses induced by magnetohydrodynamic instabilities in the ASDEX upgrade tokamak *Rev. Sci. Instrum.*, **80** 053503

[5] Zweben S J 1989 Pitch angle resolved measurements of escaping charged fusion products in TFTR *Nucl. Fusion.*, **29** 825

[6] Yang C, Stoffers C, Zhang F, Jacobsen S M, Wagner B K and Summers C J 1998 Green phosphor for low-voltage cathodoluminescent applications: $SrGa_2S_4 : Eu^{2+}$ *Appl. Phys. Lett.*, **72** 158

[7] Garcia Lopez J, Ager F J, Barbadillo Rank M, Madrigal F J, Ontalba M A, Respaldiza M A and Ynsa M D 2000 CNA: the first accelerator-based IBA facility in Spain *Nucl. Instr. Meth.*, **161-163** 1137

[8] Jimenez-Ramos M C, Garcia Lopez J, Garcia-Munoz M, Rodriguez-Ramos M, Carmona Gazquez M and Zurro B 2014 Characterization of scintillator materials for fast-ion loss detectors in nuclear fusion reactors *Nucl. Instr. Meth. Phys. Res.*, **55** 124014.

[9] Birks J B 1951 Scintillations from Organic Crystals : Specific Fluorescence and Relative Response to Different Radiations *Proc. Phys. Soc.*, A **64** 874

[10] Aberle C, Buck C, Hartmann F X, Schnert S and Wagner S 2011 Light output of Double Chooz scintillators for low energy electrons *J. Instrum.*, **6** 11

[11] Heidbrink W *et al* 2007 Alpha particle loss in the TFTR DT experiments *Plasma Phys. Control. Fusion.*, **49** 1457

[12] Galdon J *et al* 2015 The synthetic Fast Ion Loss Detector Poster at the 1st EPS Conference on Plasma Diagnostics, Frascati (Italy) (unpublished).

[13] Sieglin B A 2014 Experimental Investigation of Heat Transport and Divertor Loads of Fusion Plasma in All Metal ASDEX Upgrade and JET *Physik Department Technische Universitat Munchen.*, **Dissertation**

[14] Kurki-Suonio T *et al* 2009 ASCOT simulations of fast ion power loads to the plasma-facing components in ITER *Nucl. Fusion.*, **49** 095001

[15] Herrmann A, Eich T, Rohde V, Fuchs C J, Neuhauser J and ASDEX Upgrade team 2004 Power deposition outside the divertor in ASDEX Upgrade *Plasma Phys. Control. Fusion.*, **46** 971979

[16] Lasnier C J, Allen S L, Ellis R E, Fenstermacher M E, McLean A G, Meyer W H, Morris K, Seppala L G, Crabtree K and Van Zeeland M A 2014 Wide-angle ITER-prototype tangential infrared and visible viewing system for DIII-Da) *Rev. Sci. Instrum.*, **85** 11D855

[17] Salewski M, Nielsen S K, Bindslev H, Furtula V, Gorelenkov N N, Korsholm S B, Leipold F, Meo F, Michelsen P K, Moseev D 2011 Wide-angle ITER-prototype tangential infrared and visible viewing system for DIII-Da) *Nucl. Fusion.*, **51** 083014